Journal of Magnetism and Magnetic Materials 92 (1991) 359–365
North-Holland

Ordered magnetic frustration
XII. The magnetic structures of $Fe_3F_8(H_2O)_2$ at 40 and 2 K

M. Leblanc, G. Ferey

Laboratoire des Fluorures, URA CNRS 449, Faculté des Sciences, Route de Laval, 72017 Le Mans Cedex, France

P. Lacorre and J. Pannetier

Institut Laue–Langevin, Avenue des Martyrs, BP 156X, 38042 Grenoble Cedex, France

Received 4 June 1990

The magnetic structures of $Fe_3F_8(H_2O)_2$ are solved at 40 and 2 K from neutron powder diffraction data. At 40 K, the magnetic cell is identical with the nuclear cell ($a = 7.544(3)$ Å, $b = 7.4324(5)$ Å, $c = 7.387(3)$ Å, $\beta = 117.26(2)°$, C2/m, $Z = 2$); the Fe^{3+} magnetic moments ($\mu = 3.98(4)\mu_B$) lie along b with a G type antiferromagnetic mode while Fe^{2+} spins remain paramagnetic. At 2 K, the magnetic cell is doubled along c: ($a = 7.543(3)$ Å, $b = 7.4314(4)$ Å, $c = 14.773(5)$ Å, $\beta = 117.26(2)°$); the Fe^{3+} magnetic moments ($\mu = 4.30(12)$ μ_B) tilt apart from b axis while the Fe^{2+} spins ($\mu = 3.97(13)\mu_B$ order in the (a, c) plane. Neutron diffraction experiments confirm the "idle spin" behaviour, due to magnetic frustration, of Fe^{2+} in $Fe_3F_8(H_2O)_2$

1. Introduction

Attention has recently been paid to several 3d transition metal fluorides whe _ paramagnetic cations form triangular planes or Kagome lattices [1–12]. Most often, antiferromagnetic superexchange interactions dominate and frustration is said to occur [13].

When two different paramagnetic cations are involved in the structure, the magnetic behaviour strongly depends on the topology of the cationic subnetwork, on the cationic order or disorder and on the relative strength of the magnetic interactions.

As a result of magnetic frustration, $Fe_3F_8(H_2O)_2$ presents a very peculiar "idle spin" behaviour: as evidenced by Mössbauer spectroscopy [3], only Fe^{3+} spins order at $T_N = 157$ K while Fe^{2+} spins remain paramagnetic down to 35 K. These features can be qualitatively correlated [3] to the crystal structure of $Fe_3F_8(H_2O)_2$ (fig. 1). Indeed, the cationic subnetwork is built up from Kagome or hexagonal tungsten bronze (HTB) type layers of ordered (Fe^{2+}, $2Fe^{3+}$) cations; successive layers are related by a $0.5(a + b)$ translation. In the (002) planes, Fe^{3+} cations draw $(Fe^{3+}F_4)_2^-$ perovskite type planes connected to each other by isolated hydrated Fe^{2+} cations (fig 1), these planes are perpendicular to the preceding (HTB) planes (fig. 2).

These structural characteristics, together with weak superexchange magnetic interactions $J_{Fe^{2+}-Fe^{3+}}$, as compared with Fe^{3+}–Fe^{3+} interactions ($J_{Fe^{3+}-Fe^{3+}}$), may induce a magnetic order temperature of Fe^{2+} lower than that of Fe^{3+}.

After a brief description of the sample preparation and experimental conditions in section 2, this paper presents in section 3 a determination of the magnetic structures of $Fe_3F_8(H_2O)_2$ at 40 and 2 K. The nuclear structure will be refined first at 170 K and a comparison of $Fe_3F_8(H_2O)_2$ with isostructural $MgFe_2F_8(H_2O)_2$ will be discussed.

In a second paper [14], the magnetic structure of $Fe_3F_8(H_2O)_2$ and its magnetic behaviour will be examined by Monte Carlo simulation. These results will confirm that the magnetic structures

0304-8853/91/$03.50

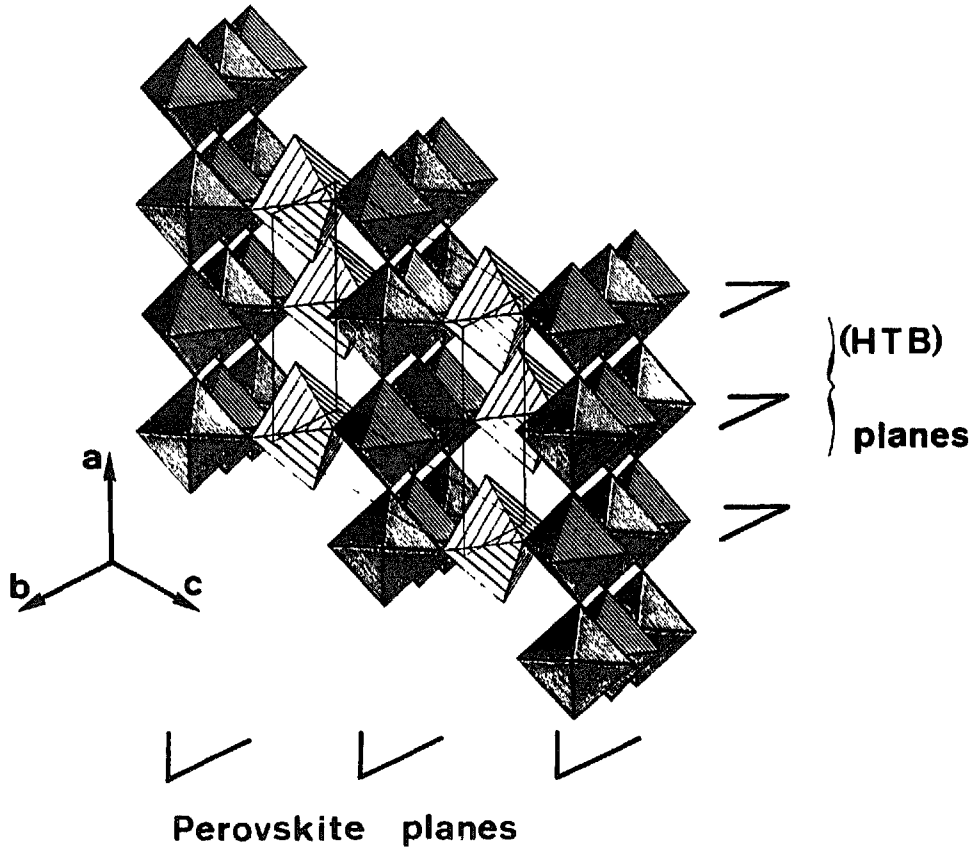

Fig 1 Perspective view of the structure of $Fe_3F_8(H_2O)_2$ in term of Fe^{2+} and Fe^{3+} octahedra (Fe^{2+} octahedra are lightly hatched)

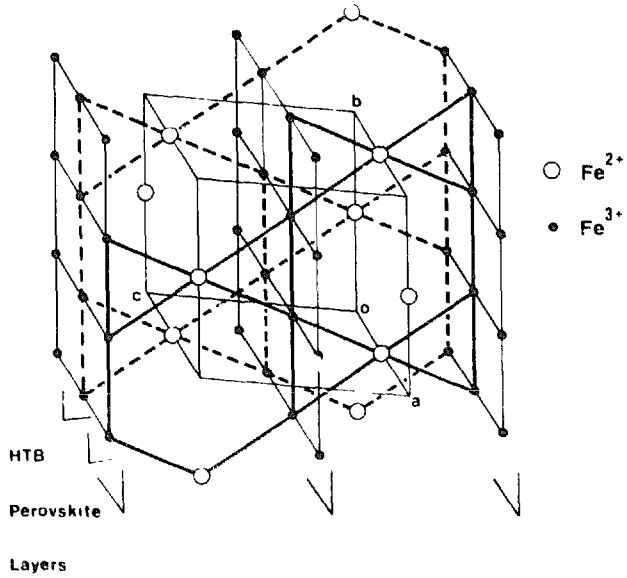

Fig 2 Perspective view of the structure of $Fe_3F_8(H_2O)_2$ in term of Kagome or perovskite type layers of Fe^{2+} and/or Fe^{3+} cations

presented in this paper are consistent with the coupling mechanisms reported in the literature.

2. Experimental

The reduction method previously described in [3] was used to grow large single crystals of $Fe_3F_8(H_2O)_2$; it was modified in order to obtain the large amounts of polycrystalline material required for neutron diffraction experiments. The hydrothermal synthesis conditions were as follows: FeF_2 (4.4×10^{-3} mol), FeF_3 (13.2×10^{-3} mol), 49% HF ($v = 1.1$ cm^3), platinum tube, filling rate $\tau = 0.7$, $T = 400\,^\circ$C, $P = 180$ MPa, $t = 50$ h.

$MgFe_2F_8(H_2O)_2$ was prepared by heating a mixture of MgF_2 (0.020 mol) and FeF_3 (0.040 mol) in 5M HF (2.20 cm^3) during 3 days at 200 °C. The

resulting light green powder was contaminated with a small amount of MgF_2.

23 neutron diffraction patterns of $Fe_3F_8(H_2O)_2$ were collected at fixed temperatures between 2 and 170 K on the powder diffractometer D1B of the Institut Laue–Langevin at Grenoble ($\lambda = 2.518$ Å, $16° \leq 2\theta \leq 96°$ at $T = 170$ K, $10° \leq 2\theta \leq 90°$ for all other patterns, 400 intensity measurements in steps of 0.2° (2θ), 25 min per pattern). A diffraction pattern of $MgFe_2F_8(H_2O)_2$ was recorded at 2.5 K in similar conditions. The powdered samples were contained in a vanadium can (10 mm diameter, $h = 40$ mm) held in a standard helium cryostat.

The diffraction patterns were analysed by using the Rietveld method [15,16]. Scattering lengths and magnetic form factors were taken from refs. [17] and [18] respectively.

3. Nuclear and magnetic structures of $Fe_3F_8(H_2O)_2$ and $MgFe_2F_8(H_2O)_2$

3.1. Nuclear structure of $Fe_3F_8(H_2O)_2$ at 170 K

The refinement of the nuclear structure of $Fe_3F_8(H_2O)_2$ was performed at 170 K. The starting set of atomic coordinates and the thermal vibration parameters (table 1) were taken from a single crystal analysis of isostructural $MnFe_2F_8(H_2O)_2$ by neutron diffraction at 200 K (D15, ILL) [19]. The final atomic coordinates and cell parameters are listed in table 1 with selected interatomic distances and angles; the reliability factors appear in table 2. The results are in good agreement with the room temperature X-ray structure determination [3,20]. The calculated Fe–F distances are very close to the sum of ionic radii [21]

Table 1
Refined cell parameters of $Fe_3F_8(H_2O)_2$ at 170, 40, 2 K and of $MgFe_2F_8(H_2O)_2$ at 2.5 K

	$Fe_3F_8(H_2O)_2$			$MgFe_2F_8(H_2O)_2$
	170 K	40 K	2 K	2.5 K
a (Å)	7.554 (4)	7.544 (3)	7.543 (3)	7.535 (8)
b (Å)	7.4428 (4)	7.4324 (5)	7.4314 (4)	7.387 (1)
c (Å)	7.391 (4)	7.387 (3)	14.773 (5)	7.531 (9)
β (°)	117.41 (3)	117.26 (2)	117.26 (2)	121.60 (5)
V (Å^3)	368.9 (5)	368.2 (4)	736.2 (6)	357.0 (9)

Refined atomic parameters of $Fe_3F_8(H_2O)_2$ at 170 K

	x	y	z	B_{iso} (Å^2)
Fe^{3+}	$\frac{1}{4}$	$\frac{1}{4}$	$\frac{1}{2}$	0.45
Fe^{2+}	0	$\frac{1}{2}$	0	0.80
F1	0	0.2992 (11)	$\frac{1}{2}$	1.20
F2	0.1781 (15)	0	0.4394 (14)	0.95
F3	0.1336 (11)	0.2962 (7)	0.2126 (8)	0.98
Ow	0.2470 (16)	0	0.0555 (16)	1.80
H	0.2090 (13)	0.1002 (11)	0.1080 (16)	2.20

Selected interatomic distances (Å) and angles (°) in $Fe_3F_8(H_2O)_2$ at 170 K

$2\times Fe^{3+}$–F1	1.924 (2)	$4\times Fe^{2+}$–F3	2.080 (5)
$2\times Fe^{3+}$–F2	1.932 (2)	$2\times Fe^{2+}$–O_w	2.131 (14)
$2\times Fe^{3+}$–F3	1.919 (5)		
$\langle d_{Fe^{3+}-F}\rangle = 1.925$			
O_w–H	0.944 (14)	H–O_w–H	104.3
H–H	1.491 (11)	O_w–H. . .F3	179.5
H F3	1.859 (12)	Fe^{3+}–F3–Fe^{2+}	141.5
O_w ..F3	2.803 (11)	Fe^{3+}–F2–Fe^{3+}	148.7
		Fe^{3+}–F1–Fe^{3+}	158.0

Table 2
Reliability factors

	$Fe_3F_8(H_2O)_2$			$MgFe_2F_8(H_2O)_2$
	170 K	40 K	2 K	2.5 K
Intensity	3.26	4.03	5.10	8.23
Profile	6.50	6.33	7.39	15.25
Weighted profile	5.34	5.33	5.68	11.75
Expected	5.32	2.68	3.59	4.63
Nuclear	3.26	3.62	4.29	8.62
Magnetic	-	5.96	7.33	7.09

of Fe^{2+} (0.78 Å) or Fe^{3+} (0.645 Å) and F^- (1.285 Å) and the geometry of the water molecule is close to that observed in similar structures [4].

3.2. Magnetic structures of $Fe_3F_8(H_2O)_2$ at 40 K and of $MgFe_2F_8(H_2O)_2$ at 2.5 K

Previous magnetization or susceptibility measurements in low applied fields [3] have shown that parasitic ferromagnetic components appear below T_N in $Fe_3F_8(H_2O)_2$ and $MgFe_2F_8(H_2O)_2$. However, the extrapolated zero field magnetizations never exceed $0.2\mu_B$ mol^{-1}; consequently, both compounds will be considered as pure antiferromagnets for neutron powder diffraction and the corresponding constraints will be applied during the refinements.

Below T_N, new magnetic peaks appear in the diffraction pattern. However, at 40 K for $Fe_3F_8(H_2O)_2$ and 2.5 K for $MgFe_2F_8(H_2O)_2$, all the new diffraction lines can be indexed in the nuclear cells (small unit cell of fig. 3).

Eight magnetic modes, foreseen by the macroscopic theory of Bertaut [22] are compatible with the space group C2/m by using three independent symmetry elements: 2_1 at ($x = \frac{1}{4}$, $z = \frac{1}{2}$), -1 at (000) and C centering. Four of them, listed in table 3 are suitable with the Fe^{3+} sublattice

The linear combinations of the magnetic moments:

$$F = M_1 + M_2 + M_3 + M_4,$$

$$G = M_1 - M_2 + M_3 - M_4,$$

$$C = M_1 + M_2 - M_3 - M_4,$$

$$A = M_1 - M_2 - M_3 + M_4,$$

represent the ferromagnetic and antiferromagnetic modes of coupling. The atomic coordinates of

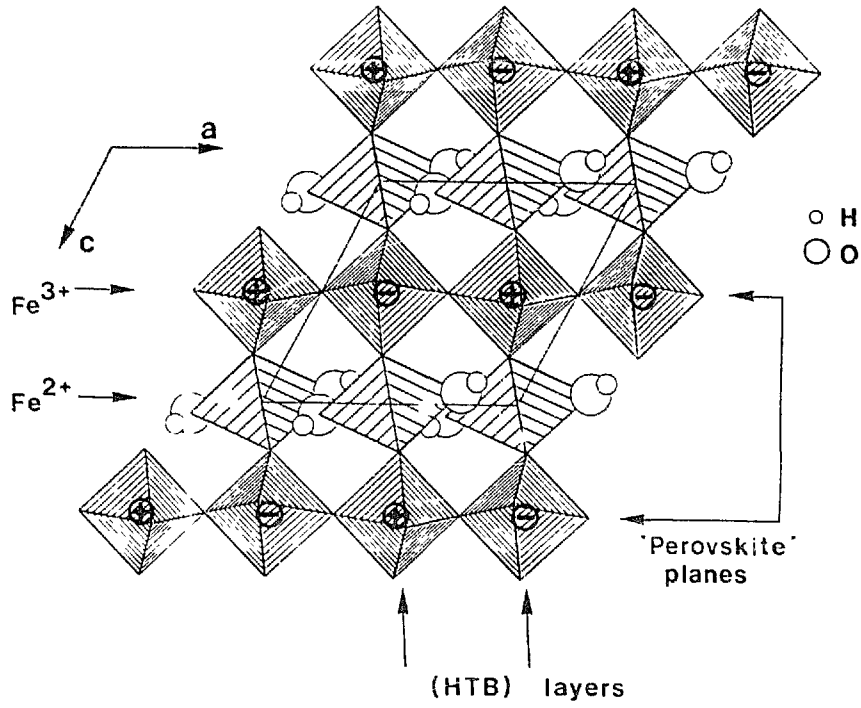

Fig. 3. Projection of the structure of $Fe_3F_8(H_2O)_2$ along b and orientation of the magnetic moments of Fe^{3+} along $\pm b$ at 40 K

Table 3
Coordinates of the magnetic cations Fe^{3+} (M_i, $i = 1, 4$) and part of the irreducible representation of Fe^{3+} in space group C2/m

M_1	$\frac{1}{4}$	$\frac{1}{4}$	$\frac{1}{2}$
M_2	$\frac{1}{4}$	$\frac{3}{4}$	$\frac{1}{2}$
M_3	$\frac{3}{4}$	$\frac{3}{4}$	$\frac{1}{2}$
M_4	$\frac{3}{4}$	$\frac{1}{4}$	$\frac{1}{2}$
Magnetic modes			
Γ_1 (+ + +)	G_x	F_y	G_z
Γ_2 (+ − −)	C_x	A_y	C_z
Γ_3 (− + +)	F_x	G_y	F_z
Γ_4 (− − −)	A_x	C_y	A_z

Fe^{3+} cations with magnetic moments M_i can be obtained from table 3.

The best fit of the observed intensities is obtained for the Γ_3 mode $F_xG_yF_z$ with $F_x = F_z = 0$ in $Fe_3F_8(H_2O)_2$ at 40 K and for the Γ_1 mode $G_xF_yG_z$ with $F_y = 0$ in $MgFe_2F_8(H_2O)_2$ at 2.5 K. The results of the refinements are given in tables 2 and 5.

Then, it is clear that the magnetic moments of Fe^{3+} lie in the plane of the perovskite type layers in $Fe_3F_8(H_2O)_2$ (fig. 3) while they are almost aligned along the normal to these planes, the [102] direction, in $MgFe_2F_8(H_2O)_2$. When viewed along this [102] axis, two successive layers present alternating moments.

The parasitic ferromagnetic components observed below T_N must lie in the (a, c) plane in $Fe_3F_8(H_2O)_2$ and along b in $MgFe_2F_8(H_2O)_2$.

3.3. Magnetic structure of $Fe_3F_8(H_2O)_2$ at 2 K

Below $T = 35$ K, new diffraction lines appear, the high-temperature c axis is doubled (large underlined cell in fig. 4) and the Bravais lattice is no longer C-centered. Fe^{2+} and/or Fe^{3+} sublattices must then present antiferromagnetic components in successive Kagome layers related by [001] and [$\frac{1}{2}$ $\frac{1}{2}$ 0] translations of the high-temperature cell. Within these hypotheses, magnetic models were sought in the (a, b, $2c$) cell by using two independent symmetry elements: -1 at (0, 0, 0) and n plane at $y = \frac{1}{4}$. The cationic positions are given in table 4.

The best agreement between observed and calculated intensities, illustrated in fig. 3, is obtained with the values of the magnetic moments (listed in table 5) of the magnetic atoms M_1 in table 4.

In the low-temperature phase, the spins of Fe^{2+} lie in the (a, c) plane at $\approx 55°$ from the a axis while the Fe^{3+} spins tilt from the b axis; the tilting angle is $\approx 20°$. In one HTB layer (fig. 4), Fe^{2+} spins adopt a ferromagnetic arrangement almost antiparallel with the components of Fe^{3+} in the (a, c) plane. Successive HTB layers along a are antiferromagnetic but an inexact compensation of the moments may give rise to the parasitic

Table 4
Coordinates and magnetic component modes of Fe^{2+} and Fe^{3+} in the low temperature magnetic structure of $Fe_3F_8(H_2O)_2$

Fe^{2+}							Fe^{3+}				
Site [a]	Position			M_x	M_y	M_z	Site	Position	M_x	M_y	M_z
1	0	$\frac{1}{2}$	0	+	+	+	1,3′	$\pm(\frac{1}{4}\ \frac{1}{4}\ \frac{1}{4})$	+	+	+
2	$\frac{1}{2}$	0	0	−	+	−	2,4′	$\pm(\frac{1}{4}\ \frac{3}{4}\ \frac{1}{4})$	+	−	+
1′	0	$\frac{1}{2}$	$\frac{1}{2}$	−	+	−	3,1′	$\pm(\frac{3}{4}\ \frac{3}{4}\ \frac{1}{4})$	−	+	−
2′	$\frac{1}{2}$	0	$\frac{1}{2}$	+	+	+	4,2′	$\pm(\frac{3}{4}\ \frac{1}{4}\ \frac{1}{4})$	−	−	−

[a] The site numbers correspond to the numbers used in table 2 of ref. [14] The prime sites are deduced from the unprimed sites by a translation of [0 0 $\frac{1}{2}$].

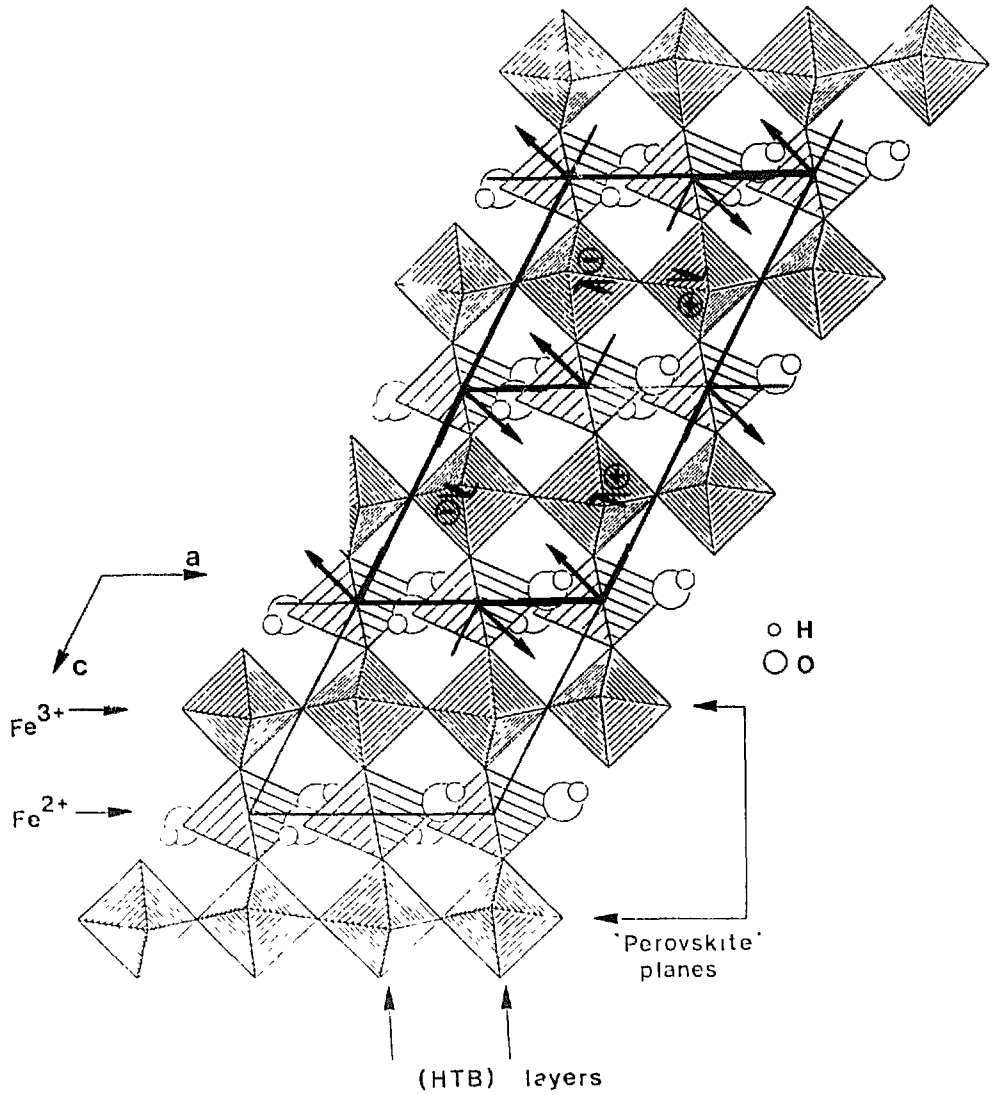

Fig. 4. Magnetic structure of $Fe_3F_8(H_2O)_2$ at 2 K.

Table 5
Refined magnetic moments (μ_B) of Fe^{3+} and Fe^{2+} in $Fe_3F_8(H_2O)_2$ at 40, 2 K and of Fe^{3+} in $MgFe_2F_8(H_2O)_2$ at 2 5 K

		M_x	M_y	M_z	M
		$Fe_3F_8(H_2O)_2$			
40 K	Fe^{3+}	0	3 98 (4)	0	3 98 (4)
	Fe^{2+}	not magnetically ordered			
2 K	Fe^{3+}	1.65 (8)	4 03 (4)	0.43 (9)	4 30 (12)
	Fe^{2+}	−4 20 (11)	0	−3 27 (17)	3 97 (13)
		$MgFe_2F_8(H_2O)_2$			
2 5 K	Fe^{3+}	2.13 (12)	0	5 39 (12)	4 40 (16)

ferromagnetic magnetization which never exceeds $0.2\mu_B$ mol^{-1} and decreases below 24 K [3,23].

4. Conclusion

The magnetic structures of $Fe_3F_8(H_2O)_2$ (T_N = 157 K) above and below the ordering temperature of Fe^{2+} were determined by neutron diffraction at 40 and 2 K respectively. Between T_N = 157 and 35 K, Fe^{3+} spins ($\mu = 3.98(4)\mu_B$ at 40 K) adopt an antiferromagnetic arrangement along the *b* axis of the monoclinic cell. In contrast, when a diamagnetic cation replaces Fe^{2+}, e.g. Mg^{2+} in $MgFe_2F_8(H_2O)_2$, Fe^{3+} spins lie along the [102] direction, perpendicular to the perovskite type planes of Fe^{3+} octahedra. It is to be noted that in $AFeF_4$ (A = K, Rb, Cs, NH_4^+) compounds, similar FeF_4^- perovskite planes are encountered; when known (A = K, Cs) [24,25], the magnetic structures are very similar to that of $MgFe_2F_8(H_2O)_2$. Then, it may reasonably assumed that the trend of Fe^{3+} moments in $Fe_3F_8(H_2O)_2$ to lie along *b*, in the perovskite type planes, comes from the influence of Fe^{2+} magnetic anisotropy.

At 2 K, Fe^{2+} ordering is achieved in $Fe_3F_8(H_2O)_2$. In one HTB layer of Fe^{2+} and Fe^{3+} octahedra, the Fe^{2+} sublattice is ferromagnetic ($\mu_{Fe^{2+}} = 3.97(13)\mu_B$ at 2 K) with spins aligned at $\approx 55°$ from the *a* axis. The Fe^{3+} sublattice is antiferromagnetic and the spins tilt apart from *b* axis ($\mu_{Fe^{3+}} = 4.30(12)\mu_B$ at 2 K). Successive HTB layers along *a* are antiferromagnetic.

This non-trivial magnetic structure is largely due to the presence of magnetic frustration in the compound. To try to get a better understanding of the magnetic behaviour of $Fe_3F_8(H_2O)_2$, we undertook a series of Monte Carlo simulations which support the results presented above. The results of these simulations will be discussed in the following paper [14].

[1] G. Ferey, M Leblanc, R. de Pape and J. Pannetier, in: Inorganic Solid Fluorides, ed. P. Hagenmuller (Academic Press, New York, 1985) p. 395.
[2] M. Leblanc, R. de Pape, G. Ferey and J. Pannetier, Solid State Commun. 58 (1986) 171.
[3] M. Leblanc, G. Ferey, Y. Calage and R de Pape, J. Solid State Chem. 53 (1984) 360.
[4] Y. Laligant, M. Leblanc, J. Pannetier and G Ferey, J Phys. C 19 (1986) 1081.
[5] Y. Laligant, J. Pannetier and G. Ferey, J. Solid State Chem. 66 (1987) 242.
[6] Y. Laligant, Y. Calage, G Heger, J. Pannetier and G Ferey, J. Solid State Chem. 78 (1989) 66.
[7] G. Ferey, R. de Pape and B. Boucher, Acta Cryst B 34 (1978) 1084.
[8] G. Ferey, M. Leblanc, R. de Pape and J. Pannetier, Solid State Commun. 53 (1985) 559.
[9] G. Ferey, R. de Pape, M. Leblanc and J. Pannetier, Rev Chim Min. 23 (1986) 474.
[10] P. Lacorre, J. Pannetier and G. Ferey, J. Magn. Magn Mat. 66 (1987) 213.
[11] P. Lacorre, M. Leblanc, J. Pannetier and G. Ferey, J Magn. Magn. Mat. 66 (1987) 219
[12] Y. Laligant, G. Ferey, G. Heger and J Pannetier, Z Anorg Allgem. Chem. 553 (1987) 163
[13] G Toulouse, Commun Phys. 2 (1977) 115
[14] P. Lacorre, J Pannetier, M. Leblanc and G Ferey, J Magn. Magn. Mat 92 (1991) 366
[15] H.M. Rietveld, J Appl. Cryst 2 (1969) 65
[16] A W Hewat, Harwell Report AERE-R7350 (1973)
[17] G Bacon, Neutron Diffraction (Clarendon Press, Oxford, 1975).
[18] R.E. Watson and A.J. Freeman, Acta Crystallogr. 14 (1961) 27.
[19] M. Leblanc, J. Pannetier and G Ferey, to be published.
[20] E Herdtweck, Z. Anorg. Allg. Chem 501 (1983) 131.
[21] R.D. Shannon, Acta Crystallogr A32 (1976) 751
[22] E.F Bertaut, in: Magnetism, vol III, eds G.T. Rado and H. Suhl (Academic Press, New York, 1963) p. 149
[23] M. Guillot, A. Marchand, M. Leblanc and G Ferey, J Phys. C 20 (1987) 2405.
[24] G Heger, R Geller and D Babel, Solid State Commun 9 (1971) 335
[25] D. Babel, F Wall and G Heger, Z Naturforsch 29b (1974) 139